Neuron
Report

SCA1-like Disease in Mice Expressing Wild-Type Ataxin-1 with a Serine to Aspartic Acid Replacement at Residue 776

Lisa Duvick,[1,2] Justin Barnes,[1,3] Blake Ebner,[1] Smita Agrawal,[1] Michael Andresen,[1] Janghoo Lim,[4,5] Glenn J. Giesler,[3] Huda Y. Zoghbi,[4] and Harry T. Orr[1,2,*]
[1]Institute of Translational Neuroscience
[2]Department of Laboratory Medicine and Pathology
[3]Department of Neuroscience
University of Minnesota, Minneapolis, MN 55455, USA
[4]Departments of Molecular and Human Genetics and Pediatrics, Howard Hughes Medical Institute, Baylor College of Medicine, Houston, TX 77030, USA
[5]Present address: Program in Cellular Neuroscience, Neurodegeneration and Repair, Department of Genetics, Yale University School of Medicine, New Haven, CT 06510, USA
*Correspondence: orrxx002@umn.edu
DOI 10.1016/j.neuron.2010.08.022

SUMMARY

Glutamine tract expansion triggers nine neurodegenerative diseases by conferring toxic properties to the mutant protein. In SCA1, phosphorylation of ATXN1 at Ser776 is thought to be key for pathogenesis. Here, we show that replacing Ser776 with a phosphomimicking Asp converted ATXN1 with a wild-type glutamine tract into a pathogenic protein. ATXN1 [30Q]-D776-induced disease in Purkinje cells shared most features with disease caused by ATXN1[82Q] having an expanded polyglutamine tract. However, in contrast to disease induced by ATXN1[82Q] that progresses to cell death, ATXN1[30Q]-D776 failed to induce cell death. These results support a model where pathogenesis involves changes in regions of the protein in addition to the polyglutamine tract. Moreover, disease initiation and progression to neuronal dysfunction are distinct from induction of cell death. Ser776 is critical for the pathway to neuronal dysfunction, while an expanded polyglutamine tract is essential for neuronal death.

INTRODUCTION

Spinocerebellar ataxia type 1 (SCA1), typically a late-onset fatal autosomal dominant neurodegenerative disease, is characterized by loss of motor coordination and balance. A prominent feature of SCA1 pathology is atrophy and loss of Purkinje cells (PCs) from the cerebellar cortex (Schut, 1950). Besides SCA1 the polyglutamine disorders include spinobulbar muscular atrophy, Huntington's disease (HD), dentatorubral-pallidoluysian atrophy, and SCAs 2, 3, 6, 7, and 17 (Orr and Zoghbi, 2007). A leading model of pathogenesis holds that the expanded polyglutamine tract alone triggers disease through an aggregation-based mechanism (Bates, 2003; Ross et al., 2003). Various data from studies on HD exemplify this concept; for example, the presence of inclusions containing mutant huntingtin N-terminal fragments including the polyglutamine stretch that correlates with disease in patients and animal models (DiFiglia et al., 1997; Gutekunst et al., 1999; Kim et al., 2001; Gray et al., 2008). Such findings support the idea that proteolysis and the generation of a polyglutamine fragment underlies the pathogenesis of HD as well as other polyglutamine disorders (Ross et al., 2003; Graham et al., 2006). However, several reports show that expansion of a glutamine tract is insufficient to cause disease (Klement et al., 1998; Katsuno et al., 2002; Emamian et al., 2003; Tsuda et al., 2005; Graham et al., 2006; Gu et al., 2009).

Recently we found that ATXN1 interacts with the RNA-binding motif protein 17 (RBM17) in a Ser776 and polyglutamine length-dependent fashion (Lim et al., 2008). Intriguingly, replacing Ser with an Asp at residue 776 increased the interaction of wild-type ATXN1[30Q] with RBM17 to a level comparable to that seen with ATXN1[82Q]-S776. Thus, by this biochemical parameter, D776 in wild-type ATXN1 generated a protein with a biochemical property of mutant ATXN1[82Q]. This raises an interesting question, what is the effect of D776 on the ability of ATXN1 to cause neurodegeneration in vivo?

RESULTS

To examine the biological relevance of D776 in ATXN1 in a mammalian model of SCA1, we generated transgenic mice expressing either *ATXN1[30Q]-D776* or *ATXN1[82Q]-D776* in cerebellar PCs (see Figures S1A and S1B available online), a major cellular site of pathology in SCA1. Since disease severity varies with levels of ATXN1 expression (Burright et al., 1995), quantitative RT-PCR and western blots were used to assess *SCA1* transgene expression in the cerebellum (Figures S1C and S1D). The *ATXN1[82Q]-D776* line with the highest level of transgene expression, line 5, was selected for detailed analysis.

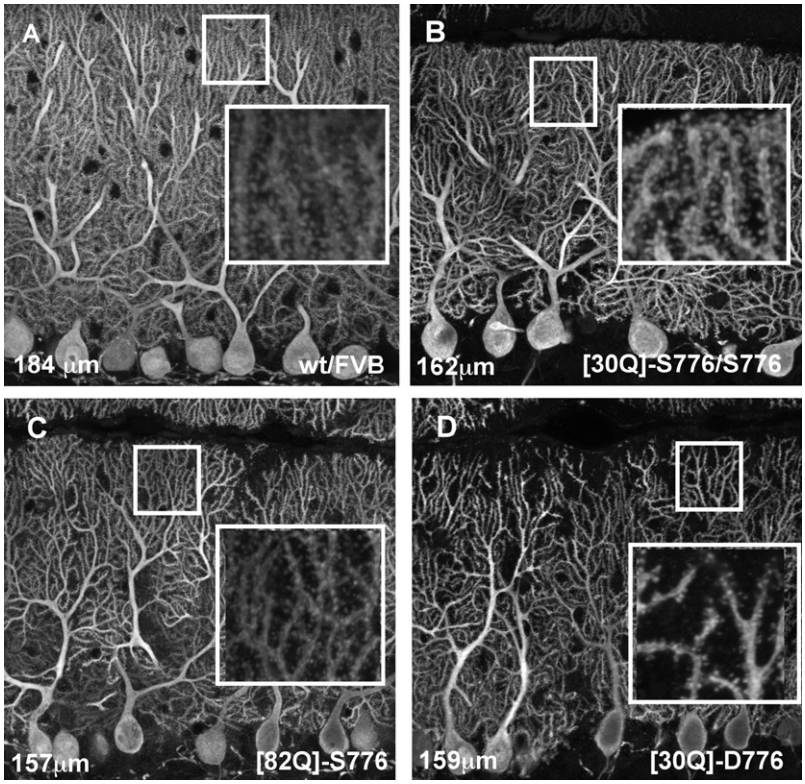

Figure 1. Atrophy of Purkinje Cell Dendrites in *ATXN1[30Q]-D776* Mice

Calbindin immunofluorescent confocal images taken at 60× with 150× enlargements (inserts) from the region of the molecular layer indicated by the white box.

(A) Purkinje cell dendritic tree of 12-week-old WT/FVB mice having a molecular layer thickness of 184 μm, ±2.6 SEM (n = 6).

(B) Purkinje cell dendritic tree of 12-week-old *ATXN1[30Q]-S776* homozygous mice having a molecular layer thickness of 162 μm, ±3.5 SEM (n = 6).

(C) Purkinje cell dendritic tree of 12-week-old *ATXN1[82Q]-S776* mice having a molecular layer thickness of 157 μm, ±2.7 SEM (n = 5).

(D) Purkinje cell dendritic tree of 12-week-old *ATXN1[30Q]-D776* mice having a molecular layer thickness of 159 μm, ±2.4 SEM (n = 4).

See also Figure S1.

This line expressed *ATXN1* mRNA at 50% of that seen in *ATXN1[82Q]-S776* line B05. *ATXN1[30Q]-D776* line 2, selected for study, expressed *SCA1* levels comparable to *ATXN1[82Q]-S776* line B05 and twice the level seen in hemizygous *ATXN1[30Q]-S776* line A02. Thus, homozygous *ATXN1[30Q]-S776* mice were used as controls for *ATXN1[30Q]-D776* mice. Figures S1D and S1E shows that transgenic protein expression in *ATXN1[30Q]-D776* and *ATXN1[30Q]-S776* homozygous mice is consistent with RNA expression levels with *ATXN1[30Q]-S776* homozygous mice expressing slightly more than *ATXN1[30Q]-D776* and *ATXN1[30Q]-S776* homozygous mice expressing slightly more ATXN1 than *ATXN1[30Q]-D776.*

We first examined whether ATXN1[30Q]-D776 induced pathology in vivo by calbindin immunostaining. In the cerebellum, calbindin is specifically expressed throughout PCs (Nakagawa et al., 1998). PCs from 12-week-old *ATXN1[30Q]-D776* mice showed considerable dendritic atrophy compared to age-matched homozygous control *ATXN1[30Q]-S776* mice (Figure 1). While the molecular layer was reduced in overall thickness to a similar degree in all of the *SCA1* mice, atrophy of the finer dendritic branches was noticeably more extensive in *ATXN1[82Q]-S776* and *ATXN1[30Q]-D776* mice. Figure 1A shows the dense deposition of PC dendrites in the molecular layer of a WT/FVB cerebellum. In the molecular layer of *ATXN1[30Q]-S776* homozygous mice there was evidence of some PC dendritic atrophy, notably some pruning of the finer dendritic branches (Figure 1B). In *ATXN1[82Q]-S776* and *ATXN1[30Q]-D776* mice, pruning of PC dendrites was even more extensive (Figures 1C and 1D, respectively), with the PC dendritic atrophy in *ATXN1[30Q]-D776* mice similar to that seen in *ATXN1[82Q]-S776* mice.

As a further pathological assessment, we examined placement of excitatory synaptic terminals onto PCs in *SCA1* mice. The two major excitatory projections to PCs, parallel fibers (PFs) and climbing fibers (CFs), segregate the sites of their terminals (Ito, 1984). While PF-PC synapses localize to the distal portions of the PC dendritic arbor, CF-PC synapses are confined to the apical dendrite and the proximal portion of the dendritic tree. Each presynaptic terminal can be defined by the expression of vesicular glutamate transporters (VGLUTs). PF terminals express VGLUT1 while CF terminals express VGLUT2 (Fremeau et al., 2001). No detectable difference in the immunostaining pattern for VGLUT1 in cerebellar sections from WT/FVB, *ATXN1[82Q]-S776*, and *ATXN1[30Q]-D776* mice was found (data not presented). Strong VGLUT1-immunoreactive puncta representing PF boutons filled the molecular layer of all three genotypes.

To assess the spatial distribution of CF terminals on PCs in the *SCA1* mice, cerebellar sections were immunostained for VGLUT2. Figure 2A shows that in 12-week-old WT/FVB mice the distribution of VGLUT2 staining extended along the primary and secondary dendrites of PCs to a mean relative height of 0.86 of the molecular layer. In 12-week-old *ATXN1[30Q]-S776* homozygous mice (Figure 2B), the mean relative height of CF terminals along PC dendrites was reduced to 0.81. In age-matched *ATXN1[82Q]-S776* mice the mean relative height of the CF terminal extension was reduced further to 0.78 (Figure 2C). Interestingly, in 12-week-old *ATXN1[30Q]-D776* mice the extension of CF terminals on PC dendrites was considerably more compromised where the CF terminals extended into the molecular layer to a mean relative height of 0.69 (Figure 2D).

Morphology of CF innervation of PCs was assessed directly by anterograde labeling of olivocerebellar projections. Injection of biotinylated dextran-amine into the contralateral inferior olive was used to visualize individual CFs and their terminals on PCs. In WT/FVB mice, as the CFs reached the inner portion of

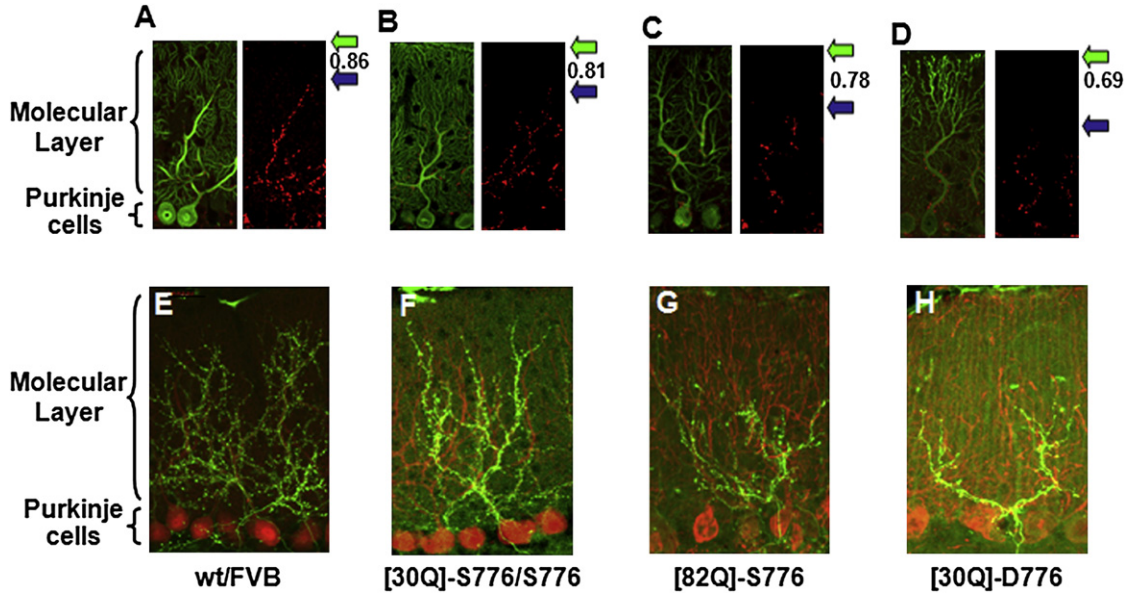

Figure 2. Altered Distribution of Climbing Fiber Terminals on Purkinje Cell Dendrites in 12-Week-Old *SCA1* Mice

(A–D) Distribution of CF terminals assessed by VGLUT2 immunostaining. Left panel is calbindin immunofluorescence (green) of Purkinje cells and right panel is VGLUT2 immunostaining (red) depicting CF terminals. (A) WT/FVB mice showing a mean relative CF to molecular layer thickness height of 0.86 ± 0.006 SEM (n = 6). (B) *ATXN1[30Q]-S776* homozygous mice with a mean relative CF to molecular layer thickness height of 0.81 ± 0.009 SEM (n = 6). (C) *ATXN1[82Q]-S776* mice having a mean relative CF to molecular layer thickness height of 0.78 ± 0.012 SEM (n = 5). (D) *ATXN1[30Q]-D776* mice with a mean relative CFs to molecular layer thickness height of 0.69 ± 0.019 SEM (n = 4).

(E–H) Distribution of CF terminals assessed by anterograde olivocerebellar projection labeling. In each panel, Purkinje cells were identified by calbindin immunofluorescence (red) and climbing fiber tracts by the presence of biotin conjugated to Alexa Fluor 488 (green) following injection into the contralateral inferior olive. (E) Distribution of CF terminals on Purkinje cells in a 12-week-old WT/FVB mouse. (F) Distribution of CF terminals on Purkinje cells in a 12-week-old *ATXN1[30Q]-S776* homozygous mouse. (G) Distribution of CF terminals on Purkinje cells in a 12-week-old *ATXN1[82Q]-S776* mouse. (H) Distribution of CF terminals on Purkinje cells in a 12-week-old *ATXN1[30Q]-D776* mouse.

See also Figure S1.

the molecular layer they gave off numerous branches that coursed along PC dendrites and extended to positions near the pial surface (Figure 2E). CFs in *ATXN1[30Q]-S776* homozygous mice had a modest level of CF pruning compared to WT/FVB animals (Figure 2F). Labeled CFs in *ATXN1[82Q]-S776* and *ATXN1[30Q]-D776* mice failed to branch to an extent seen in either WT/FVB or in *ATXN1[30Q]-S776* homozygous mice (Figures 2G and 2H, respectively). Thus, anterograde labeling of inferior olivary neurons supported the conclusion that CF arborization and extension along PC dendrites was diminished in *ATXN1[82Q]-S776* and *ATXN1[30Q]-D776* mice.

The neurological status of *ATXN1[30Q]-D776* mice was determined by measuring balance/motor coordination and gait performance. Figure 3A shows that at 6 and 12 weeks of age, *ATXN1[30Q]-D776* mice were significantly impaired on the accelerating Rotarod compared to WT/FVB and *ATXN1[30Q]-S776* homozygous mice to a degree similar to that for *ATXN1[82Q]-S776* mice (Figure 3A). Using the DigiGait system, hind stance width was evaluated since it corresponds to the broad-based gait typical of SCA1 specifically and ataxia generally in humans (Manto, 2005). As shown in Figure 3B, at 12 weeks of age the hind stance width did not significantly differ between the two control strains (WT/FVB and *ATXN1[30Q]-S776* homozygous mice). In contrast, age-matched mice from the two affected *SCA1* lines, *ATXN1[82Q]-S776* and *ATXN1[30Q]-D776* animals, had a significantly wider hind stance than age-matched littermate controls (Figure 3B). Thus, by two measures of motor performance, the ataxia in *ATXN1[30Q]-D776* mice was as severe as the ataxia in *ATXN1[82Q]-S776* mice.

A feature of disease in *ATXN1[82Q]-S776* mice is that the neurological deficit progresses with age (Clark et al., 1997). By 30 weeks of age, disease in both *ATXN1[82Q]-S776* and *ATXN1[30Q]-D776* mice progressed such that animals of both genotypes were essentially unable to perform the accelerating Rotarod task (Figure 3C). Thus, like *ATXN1[82Q]-S776* mice *ATXN1[30Q]-D776* mice also have a progressive neurological disease.

In *ATXN1[82Q]-S776* animals, pathology eventually progresses to where PCs die (Clark et al., 1997). To assess ATXN1-D776-induced disease at a late stage, we examined pathology in 1-year-old *ATXN1[30Q]-D776* and compared it to pathology in *ATXN1[82Q]-S776* animals. The molecular layer in 1-year-old WT/FVB mice was on average 170 μm thick (Figure S2A). Year-old *ATXN1[82Q]-S776* mice showed severe atrophy of PCs as quantified by molecular layer thickness as well as PC loss. The thickness of the molecular layer in these mice decreased to 123 μm in year-old animals (Figure S2B). In contrast, PC atrophy in one-year *ATXN1[30Q]-D776* mice was

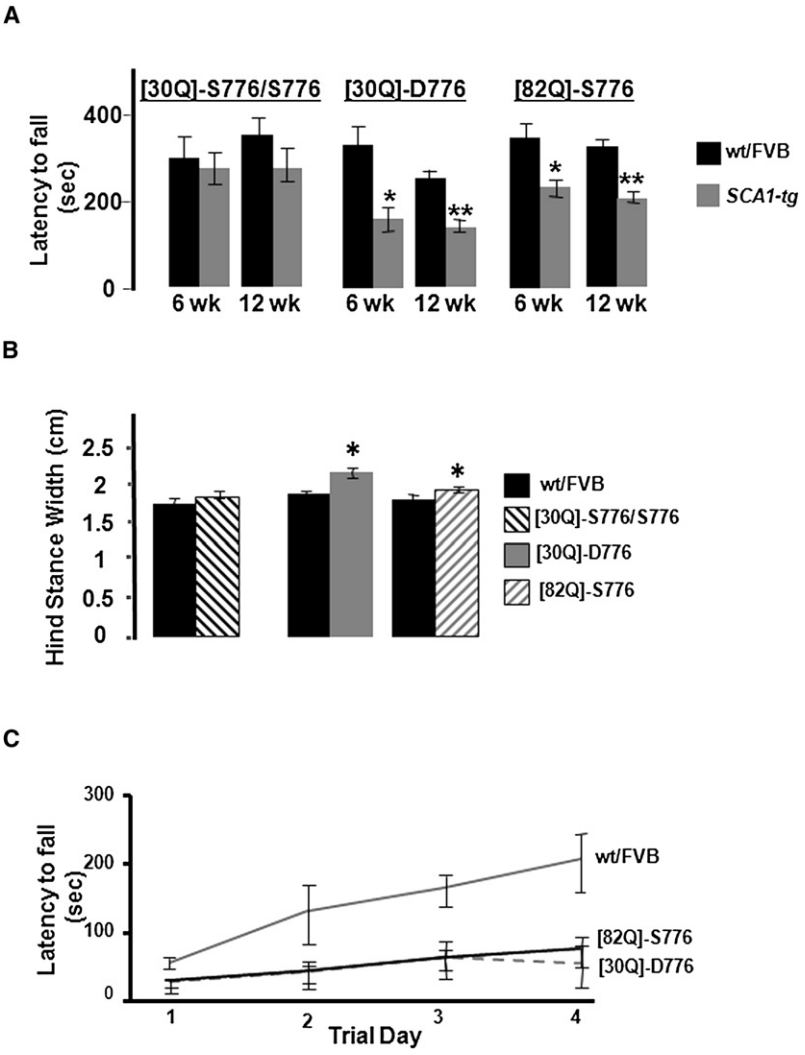

Figure 3. Altered Neurological Status of *ATXN1[30Q]-D776* Mice

(A) Accelerating Rotarod performance on day 4 at 6 and 12 weeks-of-age. *ATXN1[30Q]-S776/S776* (homozygous) mice, at 6 and 12 weeks (n = 9), were compared to age-matched WT/FVB mice, at 6 and 12 weeks (n = 10). *ATXN1[30Q]-D776* mice at 6 weeks (n = 5) and at 12 weeks (n = 14), compared to age-matched littermate WT/FVB mice at 6 weeks (n = 9) and at 12 weeks (n = 12; *p = 0.025 and **p = 0.0008, student t test, two tailed equal variance). Performance of *ATXN1[82Q]-S776* mice, at 6 weeks and 12 weeks (n = 15), compared to age-matched littermate WT/FVB mice, at 6 weeks and at 12 weeks (n = 8; *p = 0.006 and **p = 0.0005, student t test, two tailed equal variance). ±SEM.

(B) *ATXN1[30Q]-D776* mice (n = 9, *p = 0.008 student t test, two tailed equal variance) show a similar gait performance defect as *ATXN1[82Q]-S776* mice (n = 20, **p = 0.005 student t test, two tailed equal variance) compared to age-matched littermate WT/FVB mice (n = 9 &16, respectively) as assessed by hind stance width at 12 weeks-of-age. ±SEM.

(C) Four day trial of accelerating Rotarod performance of mice at 30 weeks-of-age. Both *ATXN1[30Q]-D776* (n = 3) mice and *ATXN1[82]-S776* (n = 4) at 30 weeks of age were compared to age-matched WT/FVB (n = 3) (p = 0.04 and p = 0.03). ±SEM.

See also Figure S1.

noticeably less severe. The thickness of the molecular layer of *ATXN1[30Q]-D776* mice showed little further atrophy from that seen at 12 weeks of age, decreasing from 159 μm at 12 weeks (see Figure 1D) to 148 μm at one year (Figure 4A). Thus, even though ATXN1[30Q]-D776 was able to induce neuronal dysfunction and initial dendritic atrophy similar to ATXN1[82Q]-S776, in absence of an expanded polyglutamine tract progression of dendritic atrophy was reduced considerably and disease failed to advance to neuronal cell death.

Failure of disease to induce PC death in *ATXN1[30Q]-D776* mice could be due to either the absence of an expanded polyglutamine tract or the presence of a D776. To address this, we characterized disease and its progression in animals expressing *ATXN1[82Q]-D776*. In these mice, immunostaining with the anti-ATXN1 antibody 11750 (Servadio et al., 1995) showed that ATXN1[82Q]-D776 protein was expressed in nuclei of PCs in a spatial fashion similar to the ATXN1[82Q]-S776 protein in mice from the B05 line. Consistent with the mRNA expression analysis (Figure S1C), immunostaining revealed that the expression level of ATXN1[82Q]-D776 (Figure S2C) was considerably less than ATXN1[82Q]-S776 (Figure S2D). Yet, as assessed by measuring the thickness of the molecular layer, ATXN1[82Q]-D776 induced a similar amount of PC dendritic atrophy as did ATXN1[82Q]-S776. At 12 weeks of age, the molecular layer was considerably reduced from a mean of 184 μm in age-matched wild-type mice to 147 μm in *ATXN1[82Q]-D776* mice and to 157 μm in *ATXN1[82Q]-S776* animals (Figures 4B and 4C). Neurological assessment by the accelerating Rotarod indicated that *ATXN1[82Q]-D776* mice were severely affected by 12 weeks of age (Figure 4D). Thus, it took less ATXN1[82Q]-D776 than ATXN1[82Q]-S776 to induce a similar level of disease, indicating that D776 enhanced the pathogenicity of ATXN1[82Q]. Importantly, progression of Purkinje cell atrophy was more severe in year-old *ATXN1[82Q]-D776* cerebella. The molecular layer of year-old *ATXN1[82Q]-D776* mice was on average 97 μm (Figure 4E), considerably less than 123 μm in year-old *ATXN1[82Q]-S776* cerebella (Figure S2B). Clearly, a D776 did not prevent induction of cell death and, if anything, enhanced pathology with age given that these mice expressed less ATXN1 than ATXN1[82Q]-S776 animals.

DISCUSSION

Here, we show that a single amino acid substitution outside of the polyglutamine tract converted wild-type ATXN1 into a protein, which in a mammalian model of SCA1 has many of the pathogenic capabilities of the protein with an expanded

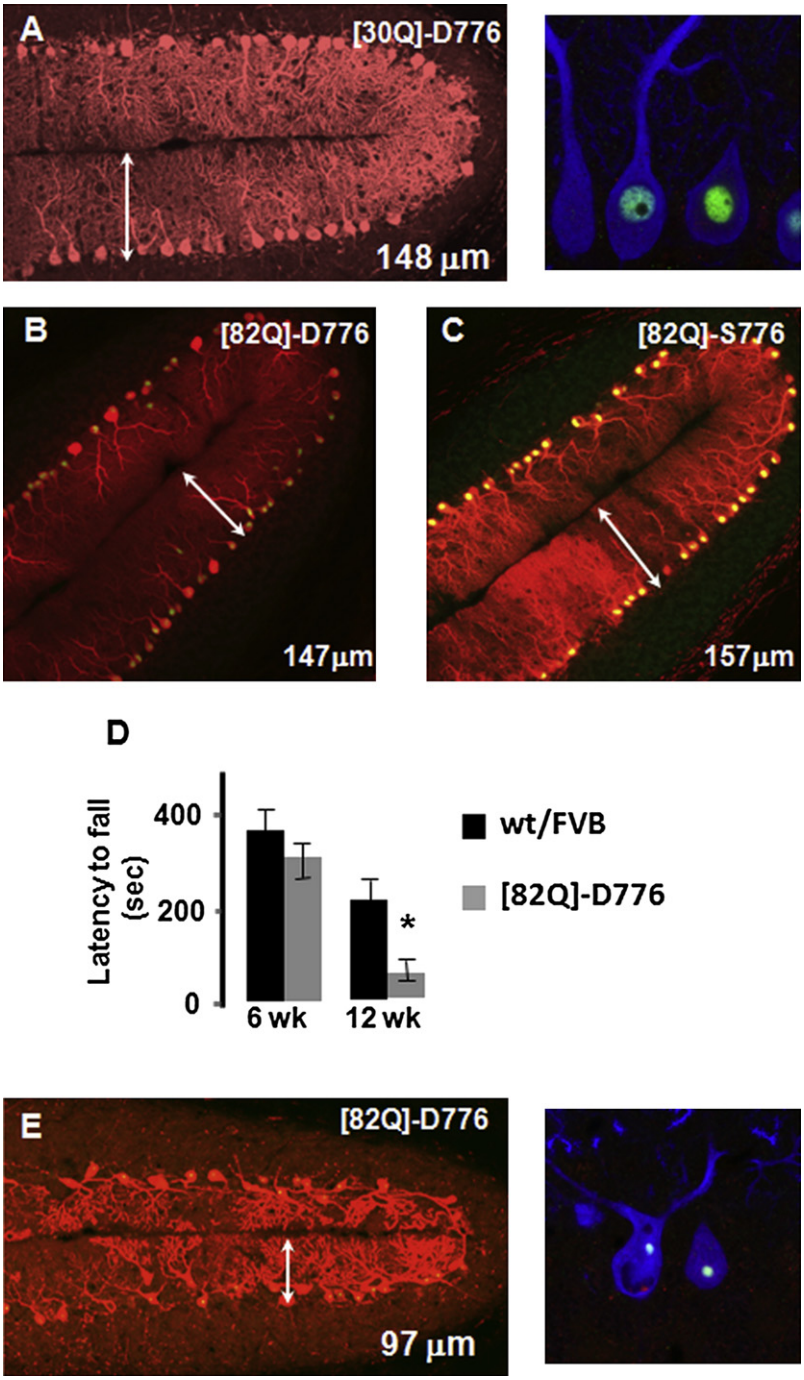

Figure 4. Cerebellar Pathology in Year-Old *SCA1* Mice

(A) Calbindin immunofluorescence of Purkinje cells in one-year-old mice expressing ATXN1[30Q]-D776 showing a molecular layer thickness of 148 ± 3.8 µm SEM (n = 3). Insert shows the absence of nuclear inclusions in PC nuclei assessed by triple immunostaining for ATXN1 (green), ubiquitin (red), and calbindin (blue). Image is a single z scan (180×).

(B) Calbindin (red) and ATXN1 (green) immunofluorescence in Purkinje cells of 12-week-old mice expressing ATXN1[82Q]-D776. Average molecular thickness was 147 ± 2.1 µm SEM (n = 3).

(C) Calbindin (red) and ATXN1 (green) immunofluorescence in Purkinje cells of 12-week-old mice expressing ATXN1[82Q]-S776. Average molecular thickness was 157 ± 2.8 µm SEM (n = 5).

(D) Accelerating Rotarod performance on day 4 of 6 (n = 12) and 12-week-old *ATXN1[82Q]-D776* (n = 5) compared to WT/FVB littermate controls, (n = 12 and 4, respectively), *p = 0.02, student t test two-tailed equal variance). ±SEM.

(E) Calbindin immunofluorescence of Purkinje cells in 1-year-old mice expressing *ATXN1[82Q]-D776* with a molecular layer thickness of 97 ± 7.0 µm SEM (n = 3). Insert depicts the presence of ubiquitin positive nuclear inclusions in PC nuclei as revealed by triple immunostaining for calbindin (blue), ATXN1 (green), and ubiquitin (red). Image is a single z scan (180×).

See also Figures S1 and S2.

polyglutamine tract. Prior studies showed that amino acids outside of the polyglutamine tract influence toxicity of a mutant polyglutamine protein (Klement et al., 1998; Katsuno et al., 2002; Emamian et al., 2003; Tsuda et al., 2005; Graham et al., 2006; Gu et al., 2009). This study demonstrates that a D776 substitution enhanced pathogenicity of ATXN1[82Q], revealing that an expanded polyglutamine tract and S776 phosphorylation have a synergistic effect on toxicity. Moreover, a D776 converted ATXN1[30Q] into a highly pathogenic protein. Thus, placing an Asp at position 776 in ATXN1 mimics pathogenic affects of polyglutamine expansion, strongly supporting a model where polyglutamine expansion has its pathogenic effect largely by altering a property associated with another region of the protein. In particular, we argue that D776 promotes the formation of ATXN1-RBM17-containing complexes that underlie some of the toxic gain of functions (Lim et al., 2008). Consistent with this idea is the observation of an increase in the amount of RBM17 in high molecular weight complexes in both *ATXN1[82Q]-S776* and *ATXN1[30Q]-D776* mice (Figure S3).

ALS nicely illustrates the concept of initiation and progression as being distinct stages of neurodegenerative disease, where evidence indicates that mutant SOD1 damage within motor neurons is linked to initiation and early stages of progression (Boillée et al., 2006). A mechanistically divergent later phase encompassing the progression to complete paralysis is coupled to the inflammatory response of microglia and mutant SOD1 toxicity within these cells (Boillée et al., 2006; Beers et al., 2006). Thus, in SOD1-induced ALS the distinct phases of disease are due to the actions of mutant protein in different cell types to produce a non-cell-autonomous killing of motor neurons. In the case of SCA1, we show that within one neuronal cell type, disease initiation and progression to neurological dysfunction can also be

distinct from later phases of disease. ATXN1[30Q]-D776 induced disease initiation and PC dysfunction. However, only in mice expressing ATXN1 with an expanded polyglutamine tract was the late-stage feature PC death seen. These results illustrate that PC death is not the cause of the neurological phenotype in SCA1 mice. The *ATXN1[30Q]-D776* mice become as neurologically compromised as *ATXN1[82Q]* mice without induction of PC death. It is worth noting that ATXN1[30Q]-D776-expressing PCs showed no sign of ATXN1 nuclear inclusions out to 1 year of age (Figure 4A). This is in contrast to *ATXN1[82Q]-D776* mice that showed PC nuclear inclusions similar to *ATXN1[82Q]-S776* animals (Figures 4E and S2B, respectively), suggesting that inclusion formation and induction of cell death require the polyglutamine expansion.

Two hypotheses for pathogenicity in the polyglutamine disorders involve (1) the generation of a toxic polyglutamine fragment (Ross et al., 2003) and (2) a toxic role of the expanded CAG repeat containing RNA (Li et al., 2008). The finding in the *ATXN1[30Q]-D776* mice that a protein is pathogenic in absence of an expanded polyglutamine tract argues against either proteolytic cleavage and the generation of a toxic polyglutamine-containing fragment or an RNA with an expanded CAG repeat as general mechanisms for polyglutamine pathogenesis. We suggest that pathogenesis can involve changes in regions of the protein in addition to the polyglutamine tract. In the case of SCA1 and ATXN1, placing an Asp at residue 776 mimics one such change.

Our finding that a phosphomimetic D776 promotes disease, combined with previous data showing that S776 is an endogenous site of phosphorylation and a phosphoresistant A776 prevents development of ataxia (Emamian et al., 2003), support the concept that S776 phosphorylation in ATXN1 drives disease initiation and development of neuronal dysfunction. Finding an inhibitor of S776 phosphorylation that suppresses disease will test this model directly as well as provide an important step toward a treatment for SCA1. It is worth noting that pathogenesis correlates with disease protein phosphorylation in other neurodegenerative diseases, e.g., α-synuclein (Fujiwara et al., 2002), and tau (Ballatore et al., 2007). More recently, substitution of phosphomimetic Asp for a Ser at residues 13 and 16 of mutant huntingtin abolished the ability of the protein to induce disease in vivo (Gu et al., 2009). Thus, targeting phosphorylation for therapeutic development may be applicable to multiple neurodegenerative diseases.

Lastly, it is worth emphasizing that beyond showing that one amino acid change can make a wild-type protein toxic we show that disease initiation and late-stage induction of neuron death are distinct phases. Obviously, the two are linked in that initiation is a prerequisite of later stages. Thus, a treatment targeted at initiation, perhaps S776 phosphorylation, is likely to have a major impact.

EXPERIMENTAL PROCEDURES

Transgenic Mice

The Institutional Animal Care and Use Committee approved all animal use protocols. Mice were housed and managed by Research Animal Resources under SPF conditions in an AAALAC-approved facility. *ATXN1[30Q]-S776* mice were from the A02 line and *ATXN1[82Q]-S776* mice from line B05 (Burright et al., 1995). The *ATXN1[30Q]-D776 and ATXN1[82Q]-D776* transgenes were generated by adding a point mutation in the original construct used to make the *ATXN1[30Q]-S776* mice. These transgenes were linearized with BamHI, gel isolated, purified by phenol/chloroform extraction, chloroform extraction, and ethanol precipitation, and suspended in injection buffer (10 mM Tris-Cl [pH 8.0]; 0.1 mM EDTA) at a concentration of 4 ng/μl. Embryo injections were performed by the Mouse Genetics Laboratory, University of Minnesota. PCR and Southern blot analyses were used to identify transgene positive animals. For *ATXN1[82Q]-D776*, eight lines were generated with five expressing the transgene all of which developed signs of disease. In the case of *ATXN1[30Q]-D776*, six lines were obtained with three expressing the transgene.

Immunostaining and Quantitative Measurements

Animals were perfused with 10% formalin and 50 μm sections were cut on a vibratome as previously described (Zu et al., 2004). Epitopes were unmasked by boiling three times for 15 s each in 0.01 M urea. The sections were blocked for 1 hr in 2% normal donkey serum and 0.3% Triton X-100 in 1× PBS. After blocking, the sections were incubated for 48 hr at 4°C in blocking solution containing primary antibody, rabbit ATXN1 11750 or 12NQ antibody at 1:2000 (Servadio et al., 1995), goat calbindin antibody (SC-7691, Santa Cruz) at 1:500, rabbit VGLUT1 antibody (135–302, Synaptic Systems) at 1:2000, or mouse VGLUT2 antibody (MAB5504, Millipore) at 1:1000 or mouse ubiquitin at 1:250 (13–1600, Invitrogen). The sections were washed 4 times in PBS and incubated for 48 hr in blocking solution containing secondary antibody. Donkey secondary Cy2, Cy3, and Cy5 were used at 1:500 (Jackson Immunoresearch). Sections were washed and mounted onto microscope slides with glycerol-gelatin (Sigma) containing 4 mg/ml n-propyl gallate. Fluorescent images were scanned using an Olympus Fluoview 1000 IX2 inverted microscope as previously described (Klement et al., 1998).

To assess the height the CF extends along the PC dendrite and the thickness of the molecular layer, 20× images were measured using Fluoview Viewer 1.7 software. Measurements of molecular layer thickness were taken on calbindin immunostained sections by measuring the distance from the base of the PC body to the end of the dendrite at the pial surface. Six measurements at the primary fissure from three cerebellar sections per animal were averaged. VGLUT2 staining was used to determine CF terminal deposition. A minimum of three animals was measured for each time point. The extension of CF terminals was depicted relative to the molecular layer thickness. Data are expressed as the mean ± SEM. The p value was calculated using Student's t test (two-tailed equal variance).

Climbing Fiber Tract Analysis—Anterograde Labeling

Animals were anesthetized with a ketamine/xylazine cocktail (100 mg ketamine and 10 mg xylazine per kg body WT) by intramuscular injection and placed into a stereotaxic frame (Model 963LS, David Kopf Instruments). The dorsal surface of the brainstem was exposed and a glass micropipette was inserted into the inferior olive. Three hundred nanoliters of 5% dextran conjugated to Alexa Fluor 488 (10,000 MW, Molecular Probes, Eugene, OR) in water was bilaterally injected using a microinjector (Model 5000, David Kopf Instruments). Five to seven days later, mice were transcardially exsanguinated with PBS (pH 7.4) and perfused with 10% formalin (25 ml). Brains were removed and fixed overnight in 10% formalin at room temperature, and placed in 30% sucrose in PBS overnight at 4°C. Cerebella were sectioned (50 μm) using a freezing sliding microtome. Purkinje cells were immunostained with anti-calbindin as described above, mounted on gelatin-coated slides, and examined using a fluorescent microscope.

Motor Performance Analyses

Accelerating Rotarod analysis was performed on 12-week-old FVB and *ATXN1[30Q]-D776* mice as described (Clark et al., 1997). Gait performance, as assessed by hind stance width, was determined using DigiGait (Mouse Specifics inc., Boston MA, USA) as described (Pallier et al., 2009). Twelve-week-old transgenic and wild-type littermates were run at 35 cm/s. The DigiGait system consists of Plexiglas housing over a clear treadmill belt. A video camera captures mice walking and 5–6 s are used for analysis.

Analysis software plots the individual paws as they contact the treadmill and calculates gait parameters. A student t test was used to show statistical significance.

SUPPLEMENTAL INFORMATION

Supplemental Information includes three figures and Supplemental Experimental Procedures and can be found with this article online at doi:10.1016/j.neuron.2010.08.022.

ACKNOWLEDGMENTS

We thank Orion Rainwater and Robert Ehlenfeldt for propagation of transgenic mouse lines and DigiGait analysis. This study was supported by NIH/NINDS grants NS062561, NS048944 (J.B.), NS (H.Y.Z.), and NS022920 and NS045667 (H.T.O.).

Accepted: July 29, 2010
Published: September 22, 2010

REFERENCES

Ballatore, C., Lee, V.M., and Trojanowski, J.Q. (2007). Tau-mediated neurodegeneration in Alzheimer's disease and related disorders. Nat. Rev. Neurosci. *8*, 663–672.

Bates, G. (2003). Huntingtin aggregation and toxicity in Huntington's disease. Lancet *361*, 1642–1644.

Beers, D.R., Henkel, J.S., Xiao, Q., Zhao, W., Wang, J., Yen, A.A., Siklos, L., McKercher, S.R., and Appel, S.H. (2006). Wild-type microglia extend survival in PU.1 knockout mice with familial amyotrophic lateral sclerosis. Proc. Natl. Acad. Sci. USA *103*, 16021–16026.

Boillée, S., Yamanaka, K., Lobsiger, C.S., Copeland, N.G., Jenkins, N.A., Kassiotis, G., Kollias, G., and Cleveland, D.W. (2006). Onset and progression in inherited ALS determined by motor neurons and microglia. Science *312*, 1389–1392.

Burright, E.N., Clark, H.B., Servadio, A., Matilla, T., Feddersen, R.M., Yunis, W.S., Duvick, L.A., Zoghbi, H.Y., and Orr, H.T. (1995). SCA1 transgenic mice: a model for neurodegeneration caused by an expanded CAG trinucleotide repeat. Cell *82*, 937–948.

Clark, H.B., Burright, E.N., Yunis, W.S., Larson, S., Wilcox, C., Hartman, B., Matilla, A., Zoghbi, H.Y., and Orr, H.T. (1997). Purkinje cell expression of a mutant allele of SCA1 in transgenic mice leads to disparate effects on motor behaviors, followed by a progressive cerebellar dysfunction and histological alterations. J. Neurosci. *17*, 7385–7395.

DiFiglia, M., Sapp, E., Chase, K.O., Davies, S.W., Bates, G.P., Vonsattel, J.P., and Aronin, N. (1997). Aggregation of huntingtin in neuronal intranuclear inclusions and dystrophic neurites in brain. Science *277*, 1990–1993.

Emamian, E.S., Kaytor, M.D., Duvick, L.A., Zu, T., Tousey, S.K., Zoghbi, H.Y., Clark, H.B., and Orr, H.T. (2003). Serine 776 of ataxin-1 is critical for polyglutamine-induced disease in SCA1 transgenic mice. Neuron *38*, 375–387.

Fremeau, R.T., Jr., Troyer, M.D., Pahner, I., Nygaard, G.O., Tran, C.H., Reimer, R.J., Bellocchio, E.E., Fortin, D., Storm-Mathisen, J., and Edwards, R.H. (2001). The expression of vesicular glutamate transporters defines two classes of excitatory synapse. Neuron *31*, 247–260.

Fujiwara, H., Hasegawa, M., Dohmae, N., Kawashima, A., Masliah, E., Goldberg, M.S., Shen, J., Takio, K., and Iwatsubo, T. (2002). alpha-Synuclein is phosphorylated in synucleinopathy lesions. Nat. Cell Biol. *4*, 160–164.

Graham, R.K., Deng, Y., Slow, E.J., Haigh, B., Bissada, N., Lu, G., Pearson, J., Shehadeh, J., Bertram, L., Murphy, Z., et al. (2006). Cleavage at the caspase-6 site is required for neuronal dysfunction and degeneration due to mutant huntingtin. Cell *125*, 1179–1191.

Gray, M., Shirasaki, D.I., Cepeda, C., André, V.M., Wilburn, B., Lu, X.H., Tao, J., Yamazaki, I., Li, S.H., Sun, Y.E., et al. (2008). Full-length human mutant huntingtin with a stable polyglutamine repeat can elicit progressive and selective neuropathogenesis in BACHD mice. J. Neurosci. *28*, 6182–6195.

Gu, X., Greiner, E.R., Mishra, R., Kodali, R., Osmand, A., Finkbeiner, S., Steffan, J.S., Thompson, L.M., Wetzel, R., and Yang, X.W. (2009). Serines 13 and 16 are critical determinants of full-length human mutant huntingtin induced disease pathogenesis in HD mice. Neuron *64*, 828–840.

Gutekunst, C.A., Li, S.H., Yi, H., Mulroy, J.S., Kuemmerle, S., Jones, R., Rye, D., Ferrante, R.J., Hersch, S.M., and Li, X.J. (1999). Nuclear and neuropil aggregates in Huntington's disease: relationship to neuropathology. J. Neurosci. *19*, 2522–2534.

Ito, M. (1984). The Cerebellum and Neural Control (New York: Raven Press).

Katsuno, M., Adachi, H., Kume, A., Li, M., Nakagomi, Y., Niwa, H., Sang, C., Kobayashi, Y., Doyu, M., and Sobue, G. (2002). Testosterone reduction prevents phenotypic expression in a transgenic mouse model of spinal and bulbar muscular atrophy. Neuron *35*, 843–854.

Kim, Y.J., Yi, Y., Sapp, E., Wang, Y., Cuiffo, B., Kegel, K.B., Qin, Z.H., Aronin, N., and DiFiglia, M. (2001). Caspase 3-cleaved N-terminal fragments of wild-type and mutant huntingtin are present in normal and Huntington's disease brains, associate with membranes, and undergo calpain-dependent proteolysis. Proc. Natl. Acad. Sci. USA *98*, 12784–12789.

Klement, I.A., Skinner, P.J., Kaytor, M.D., Yi, H., Hersch, S.M., Clark, H.B., Zoghbi, H.Y., and Orr, H.T. (1998). Ataxin-1 nuclear localization and aggregation: role in polyglutamine-induced disease in SCA1 transgenic mice. Cell *95*, 41–53.

Li, L.-B., Yu, Z., Teng, X., and Bonini, N.M. (2008). RNA toxicity is a component of ataxin-3 degeneration in Drosophila. Nature *453*, 1107–1111.

Lim, J., Crespo-Barreto, J., Jafar-Nejad, P., Bowman, A.B., Richman, R., Hill, D.E., Orr, H.T., and Zoghbi, H.Y. (2008). Opposing effects of polyglutamine expansion on native protein complexes contribute to SCA1. Nature *452*, 713–718.

Manto, M.-U. (2005). The wide spectrum of spinocerebellar ataxias (SCAs). Cerebellum *4*, 2–6.

Nakagawa, S., Watanabe, M., Isobe, T., Kondo, H., and Inoue, Y. (1998). Cytological compartmentalization in the staggerer cerebellum, as revealed by calbindin immunohistochemistry for Purkinje cells. J. Comp. Neurol. *395*, 112–120.

Orr, H.T., and Zoghbi, H.Y. (2007). Trinucleotide repeat disorders. Annu. Rev. Neurosci. *30*, 575–621.

Pallier, P.N., Drew, C.J., and Morton, A.J. (2009). The detection and measurement of locomotor deficits in a transgenic mouse model of Huntington's disease are task- and protocol-dependent: influence of non-motor factors on locomotor function. Brain Res. Bull. *78*, 347–355.

Ross, C.A., Poirier, M.A., Wanker, E.E., and Amzel, M. (2003). Polyglutamine fibrillogenesis: the pathway unfolds. Proc. Natl. Acad. Sci. USA *100*, 1–3.

Schut, J.W. (1950). Hereditary ataxia: clinical study through six generations. Arch. Neurol. Psychiatry *63*, 535–568.

Servadio, A., Koshy, B., Armstrong, D., Antalffy, B., Orr, H.T., and Zoghbi, H.Y. (1995). Expression analysis of the ataxin-1 protein in tissues from normal and spinocerebellar ataxia type 1 individuals. Nat. Genet. *10*, 94–98.

Tsuda, H., Jafar-Nejad, H., Patel, A.J., Sun, Y., Chen, H.K., Rose, M.F., Venken, K.J., Botas, J., Orr, H.T., Bellen, H.J., and Zoghbi, H.Y. (2005). The AXH domain of Ataxin-1 mediates neurodegeneration through its interaction with Gfi-1/Senseless proteins. Cell *122*, 633–644.

Zu, T., Duvick, L.A., Kaytor, M.D., Berlinger, M.S., Zoghbi, H.Y., Clark, H.B., and Orr, H.T. (2004). Recovery from polyglutamine-induced neurodegeneration in conditional SCA1 transgenic mice. J. Neurosci. *24*, 8853–8861.